NeuroImage: Clinical 25 (2020) 102103

Contents lists available at ScienceDirect

NeuroImage: Clinical

journal homepage: www.elsevier.com/locate/ynicl

Imaging the Nigrosome 1 in the substantia nigra using susceptibility weighted imaging and quantitative susceptibility mapping: An application to Parkinson's disease

Zenghui Cheng[a,1], Naying He[a,1], Pei Huang[b,1], Yan Li[a], Rongbiao Tang[a], Sean K. Sethi[c,d], Kiarash Ghassaban[d,e], Kiran Kumar Yerramsetty[f], Vinay Kumar Palutla[f], Shengdi Chen[b,*], Fuhua Yan[a,*], E. Mark Haacke[a,b,c,d,e]

[a] Department of Radiology, Ruijin Hospital, Shanghai Jiao Tong University School of Medicine, 197 Ruijin Er Road, Shanghai, 200025, China
[b] Department of Neurology, Ruijin Hospital, Shanghai Jiao Tong University School of Medicine, 197 Ruijin Er Road, Shanghai, 200025, China
[c] Magnetic Resonance Innovations, Inc, 30200 Telegraph Road, Bingham Farms, MI, 48025, USA
[d] Department of Radiology, Wayne State University, 42 W. Warren Ave. Detroit, MI, 48202, USA
[e] Department of Biomedical Engineering, Wayne State University, 42 W. Warren Ave. Detroit, MI, 48202, USA
[f] MR Medical Imaging Innovations India Pvt. Ltd, Flat No.401, Plot No.397, SAI HOUSE, Ayyappa Society, Madhapur, Hyderabad, Telangana, 500081, India

ARTICLE INFO

Keywords:
Substantia nigra
Nigrosome 1
Swallowtail sign
Susceptibility weighted imaging
Susceptibility mapping
Iron content

ABSTRACT

Parkinson's disease (PD) is a clinically heterogeneous chronic progressive neuro-degenerative disease with loss of dopaminergic neurons in the nigrosome 1 (N1) territory of the substantia nigra pars compacta (SNpc). To date, there has been a major effort to identify changes in the N1 territory by monitoring increases of iron in the SNpc. However, there is no standard protocol being used to visualize or characterize the N1 territory. Therefore, the purpose of this study was to create a robust high quality, rapid imaging protocol, determine a slice by slice characterization of the appearance of N1 (the "N1 sign") and evaluate the loss of the N1 sign in order to differentiate healthy controls (HCs) from patients with PD. Firstly, one group of 10 HCs was used to determine the choice of imaging parameters. Secondly, another group of 80 HCs was used to characterize the appearance of the N1 sign and train the raters. In this step, the magnitude, susceptibility weighted images (SWI), quantitative susceptibility maps (QSM) and true SWI (tSWI) images were all reviewed using data from a 3D gradient recalled echo sequence. A resolution of 0.67 mm × 0.67 mm × 1.34 mm was chosen based on the ability to cover all the basal ganglia, midbrain and dentate nucleus with good signal-to-noise with echo times of 11 ms and 20 ms. Thirdly, 80 Parkinsonism and related disorders patients [idiopathic Parkinson's disease (IPD): 57; atypical parkinsonian syndromes (APs): 14; essential tremor (ET): 9] and one additional group of 80 age-matched HCs were blindly analyzed for the presence or absence of the N1 sign for a differential diagnosis. From the first group of 80 HCs, all of the 76 (100%) cases (4 were excluded due to motion artifacts) showed the N1 sign in one form or another after reviewing the first 5 caudal slices of the SN. For the second group of 80 HCs, 78 (97.5%) showed the N1 sign in at least 2 slices. Of the 80 Parkinsonism and related disorders patients, 32 (56.1%, 32/57) IPD and 6 (42.9%, 6/14) APs showed a bilateral loss of the N1 sign, 12 (21.1%, 12/57) IPD and 6 (42.9%, 6/14) APs showed the N1 sign unilaterally and 13 (22.8%, 13/57) IPD and 2 (14.2%, 2/14) APs showed the N1 sign bilaterally. Also, all 9 (100%, 9/9) ET patients showed the N1 sign bilaterally. The mean total structure and mean high susceptibility region for the SN for both IPD and APs patients with bilateral loss of N1 were higher than those of the HCs ($p < 0.002$). In conclusion, the N1 sign can be consistently visualized using tSWI with a resolution of at least 0.67 mm × 0.67 mm × 1.34 mm and can be seen in 95% of HCs.

PD -	Parkinson's Disease	NM -	Neuromelanin
IPD-	idiopathic Parkinson's disease	SNPc -	Substantia Nigra Pars Compacta
N1 -	Nigrosome 1	DNH -	dorsal-nigral hyperintensity

* Corresponding authors.
E-mail address: yfh11655@rjh.com.cn (F. Yan).
[1] All these three authors made equal contributions.

https://doi.org/10.1016/j.nicl.2019.102103
Received 17 May 2019; Received in revised form 14 October 2019; Accepted 18 November 2019
Available online 20 November 2019

HCs - Healthy Controls
QSM - Quantitative Susceptibility Mapping
SWI - Susceptibility Weighted Imaging
tSWI - True Susceptibility Weighted Imaging
ET - Essential Tremor
APs - atypical Parkinsonism syndromes
STS - Swallowtail Sign
T2*WI - T2* Weighted Imaging
SMWI - Susceptibility Map-weighted Imaging
TE - echo time
SNR - Signal to Noise Ratio
GRE - Gradient Echo
MDS - Movement Disorder Society
MSA - Multisystem Atrophy
PSP- Progressive Supranuclear Palsy
MMSE - Mini-Mental State Examination
FA - Flip Angle
TR - Resolution Time
BW - Bandwidth
ROI - Region of Interest
mIP - Minimum Intensity Projection
MTC - magnetization transfer contrast
BLN1 - Bilateral Loss of the N1 Sign
ULN1- Unilateral Loss of the N1 Sign
BN1 - Bilateral N1 Sign
RII - High-iron thresholded region
iSWIM - Iterative Susceptibility Weighted Imaging and Mapping
TH - Slice Thickness
THo - Slice Thickness of the Reference Scan
CNR - Contrast to Noise Ratio

1. Introduction

Parkinson's disease (PD) is a chronic progressive neurodegenerative disease. It is more common in middle-aged and elderly people. In 2015, the number of PD patients in the world was estimated to be 6.2 million (Vos et al., 2016). The prevalence in China is 1.7% among people over 65 years old (Zhang et al., 2005). The disease develops over many years and in the end has a high disability rate. At present, there is still a paucity of clinically validated biomarkers for the diagnosis of PD and its accurate diagnosis depends on the ability of the clinician to identify its characteristic signs and related symptoms. Practically, PD is heterogeneous in terms of its motor symptoms, non-motor symptoms, and progression of the disease with underlying different neuropathologic changes (Thenganatt and Jankovic, 2014). The clinical heterogeneity of PD further increases the difficulty of differential diagnosis between idiopathic Parkinson's disease (IPD), atypical parkinsonian syndromes (APs) and other related disorders (for example, essential tremor (ET)) prompting people to try and find objective biological markers that can reflect the pathophysiological changes of the disease to assist in early diagnosis of IPD and predict disease prognosis.

It is well known that there is a loss of dopaminergic neurons in the substantia nigra pars compacta (SNpc). There are clusters (called nigrosomes) of high concentrations of neuromelanin (NM) distributed non-uniformly throughout the SNpc (Damier et al., 1999a). The nigrosome 1 (N1) appears to be the largest and is located in the dorsal medial aspect of the tail (caudal most part) of the SNpc. NM is composed of melanin, metal ions, lipids and proteins. Melanin binds to a large number of metal ions, providing neuroprotective effects against metal toxicity (Zecca et al., 2008; Zucca et al., 2017) of which iron ions are the most abundant (Zecca et al., 2001, 2004). The NM released from degenerating neurons to the outside of the cell attracts activated microglia and triggers a chronic inflammatory response in the SNpc. Histological studies have shown that NM-rich dopaminergic neuronal cell degeneration occurs in the tail and lateral part of the SNpc in the N1 territory first, and then the lateral and head parts in N2, N4, N3 and N5 as the disease progresses (Damier et al., 1999b). Imaging studies have also found that increased iron deposition occurs in the SNpc in PD patients (Lehericy et al., 2014). The disappearance of N1 in magnetic resonance imaging (MRI) is known to occur over time and is thought to be associated with an increase in iron deposition (Schwarz et al., 2018). This N1 sign is a potential imaging biomarker of pathophysiologic changes in PD patients.

However, the identification of the N1 sign is still rather subjective and depends on the scanning parameters and imaging sequences that are used (Blazejewska et al., 2013). The N1 sign has been described as two hypointense tails with a hyperintense middle [the so called "swallowtail sign (STS)"] on T2* weighted imaging (T2*WI) or susceptibility weighted imaging (SWI) data (Schwarz et al., 2014). Other papers have recognized it as an ovoid sign (Blazejewska et al., 2013) or dorsal-nigral hyperintensity (DNH) sign (Reiter et al., 2015) in either magnitude or SWI data because in high resolution images the two tails are connected posteriorly.

Recently, quantitative susceptibility mapping (QSM) has been used to study iron content of the deep gray matter and, particularly, in PD studies of the SN (He et al., 2017, 2015). QSM is believed to be more sensitive than R2* (1/T2*), which has been until recently the prevailing method for assessing iron in PD (Du et al., 2016; He et al., 2015; Langkammer et al., 2016). However, most studies focused on the average change in iron deposition content over the whole SN; but little is known about its distribution in the SN or SNpc. Some recent work has noted that the abnormal deposition of iron in PD patients is not evenly distributed throughout the SN structure (Schmidt et al., 2017). Since T2*WI and SWI data have little signal change for small amounts of iron and short echo times, they can fail to show the N1 sign. One group (Nam et al., 2017) used QSM and a modified form of SWI referred to as true SWI (tSWI) (Liu et al., 2014) or susceptibility map-weighted imaging (SMWI) to enhance the contrast of iron containing regions.

Another recent paper used the proportion of voxels with susceptibility less than 70 ppb as a marker of the N1 sign to distinguish PD patients (n = 38) from healthy controls (HCs (n = 25)). They found that a proportion threshold of 1.9% yielded 100% sensitivity and 100% specificity, which was not only better than the mean susceptibility value, but also visual assessment based on SMWI (Kim et al., 2018). However, a study in 2017 (Schmidt et al., 2017) showed that for the 7T SWI data of 13 HCs, there was poor agreement between raters in finding the N1 sign. For the three raters who participated in the study, the positive predictive values were 100%, 45%, and 83% while the accuracy was 100%, 77%, and 96%, respectively. They noted that even in HCs, the N1 sign showed significant individual differences, which might also affected by the adjacent other nigrosomes including N3 and N4, again highlighting the need to better characterize the N1 sign from slice to slice.

A few other weaknesses of previous works identifying the N1 sign include (Mahlknecht et al., 2017; Pavese and Tai, 2018): the small number of cases collected, the long data acquisition times, the lack of a standardized interpretation of the N1 sign, and the lack of an optimized choice of resolution and echo time. Consistent recognition of the N1 sign among raters has been difficult due to individual differences in the shape of the N1 territory and to the choice of imaging parameters such as: scanning plane, resolution, signal-to-noise (SNR) and echo time (Kim et al., 2018; Schmidt et al., 2017). Two critical elements needed to adopt the use of the N1 sign is a characterization of the appearance of N1 and a set of rules by which to draw conclusions for the presence or absence or partial presence of any nigrosome sign. The current lack of a full 3D characterization of the N1 and rules to identify it leads to an inconsistent interpretation of the data. Therefore, there is a clear need for reproducible and standardized MR protocols as well as a systematic evaluation of the N1 visibility.

In this work, we chose: first, to determine the optimal resolution, echo time and flip angle for the 3D recalled gradient echo (GRE) imaging sequence; second, to create a slice by slice characterization of the

appearance of N1 from a set of HCs; third, to differentiate PD patients from HCs; and fourth, to determine if the loss of the N1 sign in PD patients is associated with an increase in local iron content in the SN.

2. Materials and methods

2.1. Subjects

This study was approved by the local Institutional Review Board and all subjects signed a consent form. Eighty (80) patients including IPD, APs and ET were recruited and diagnosed by two of the authors (SC, PH, 30 years and 7 years of experience in movement disorders diagnosis, respectively) in consensus during the period from May 2018 to November 2018. All the PD patients were assessed using the severity of motor symptoms based on the Hoehn & Yahr stage (Hoehn and Yahr, 1967) and UPDRS-III by another one of the authors (PH). The diagnosis of IPD was based on the Movement Disorder Society (MDS) PD criteria (Postuma et al., 2015). The diagnosis of APs including multisystem atrophy (MSA) and progressive supranuclear palsy (PSP) was based on the American Academy of Neurology and American Autonomic Society (Gilman et al., 1999) and the NINDS-PSP criteria (Litvan et al., 1996), respectively. The diagnosis of ET was based on the MDS on Tremor consensus (Deuschl et al., 1998). The exclusion criteria were as follows: (1) dementia: Mini-Mental State Examination (MMSE) score < 24; (2) a history of cerebrovascular disease (e.g., infarction, hemorrhage), brain tumor, head trauma or any other type of psychiatric disorders; (3) a history of medication known to cause parkinsonism or affect clinical assessment; (4) contraindications to an MRI examination. and (5) younger than 40 years. One hundred and seventy (170) age-matched HCs were recruited from our Institutional Review Board according to the following inclusion criteria: (1) older than 40 years, without family history of movement disorders; (2) without any neurological or psychiatric disorders; and (3) a MMSE score of at least 24. Of the 170 HCs, there were 10 HCs for optimization of scan parameters, 80 HCs for assessment and characterization of the N1 sign, and another 80 HCs for testing the use of the N1 sign in PD diagnosis.

2.2. MR scanning

All imaging took place on two Philips 3T scanners (Ingenia, Philips Healthcare, Eindhoven, The Netherlands) with the same 15-channel head coil. The first 4 HCs were scanned to evaluate the effects of flip angle (FA) change. The next 6 HCs were scanned to determine optimal resolution and echo time using a 3D gradient echo sequence to delineate the N1 territory. The next 240 subjects were all scanned identically with the final protocol. The first set of age matched 80 HCs scanned was used to characterize the N1 sign and train the readers. The following 80 Parkinsonism and related disorders patients and the second set of age matched 80 HCs were used in a blinded analysis of the N1 territory. All imaging scans were acquired along the anterior commissure-posterior commissure (AC-PC) line.

2.3. Scan parameters for preliminary assessment of the N1 Sign in 10 HCs with varying flip angle, echo time and resolution:

For the first 4 HCs, a resolution of 0.67 mm × 0.67 mm × 1 mm was used with two FAs of 6° and 9°. These two values were chosen for the following reasons: first, 6° provides a spin density weighted image of gray matter, white matter and blood and will have no pulsatile artifacts. Second, a flip angle of 9° was chosen from the lesser of the Ernst angles values of 13.4°, 10.2° and 9° for white matter (T1 = 950 ms), gray matter (T1 = 1650 ms) and blood (T1 = 2000 ms) to minimize pulsatile artifacts but maximize signal-to-noise. Then, 6 HCs were evaluated as follows to choose the best image quality via resolution and SNR considerations: a) *resolution:* 0.67 mm × 0.67 mm × 1.34 mm, 0.67 mm × 0.67 mm × 1 mm and 0.67 mm × 0.67 mm × 0.67 mm all with a bandwidth (BW) = 144.7 Hz/pixel, and b) *echo time:* two echoes with TE1 = 11 ms and TE2 = 20 ms, an FA of 9° and a TR of 26 ms. All scans used the same FOV = 256 mm x 192 mm, an in-plane resolution of 0.67 mm x 0.67 mm and a parallel imaging factor of 2.4 to provide for rapid scanning, 5 min, 48 s.

2.4. Preliminary assessment to characterize the N1 sign

In order to assess the best SNR, regions-of-interest (ROIs) were drawn in the most uniform part of the white matter in the cranial aspects of the brain on the first echo magnitude data. These ROIs were drawn in the same area for each image set using SPIN software (SpinTech, Inc, Bingham Farms, MI, USA). Mean and standard deviation for each ROI was recorded and compared for each resolution and FA. The seven-echo data magnitude and QSM data were assessed visually for image quality.

2.5. Final imaging protocol

In addition to the standard clinical sequences, the final high resolution GRE scan was run with the following imaging parameters: a flip angle of 9°, a resolution of 0.67 mm × 0.67 mm × 1.34 mm, a BW of 217 Hz/pixel and two echoes of 11 ms and 20 ms. This offers high resolution T2*WI, SWI, QSM and tSWI data (Liu et al., 2014) with good brain coverage and good SNR in a reasonable period of time (5 min and 48 s).

2.6. Image post-processing for the GRE data

The phase from each echo was processed using iterative susceptibility weighted imaging and mapping (iSWIM) as the QSM reconstruction algorithm (Tang et al., 2013). This thresholded k-space technique was implemented using SPIN software (SpinTech, Inc., Bingham Farms, MI, USA). QSM data was created for both echoes.

To review the N1 territory, four types of images were generated: the original T2*WI magnitude images, SWI data, QSM data (for both echoes) and tSWI. The tSWI data was created using a mask from the QSM data to enhance the contrast in the original magnitude data (Liu et al., 2014). The reason for using tSWI is that it does not have the orientation dependence inherent in the phase data which negatively affects the SWI data. To compare the images with different slice thickness (TH), minimum intensity projections (mIP) were used to create images over roughly the same TH when viable. For this evaluation, the structure of the SN was reviewed from the most caudal to most cranial portions abutting the sub-thalamic nucleus. More specifically, the visibility of the N1 sign was reviewed in the most caudal 5 slices covering roughly 7 mm from the lower part of the SN up to the lower/middle part of the red nucleus.

2.7. Characterizing the N1 sign throughout the SN

All data were reviewed by four of the authors (EMH, 35 years of experience in MR imaging; ZC, 10 years of experience in diagnostic imaging; NH, 7 years of experience in diagnostic imaging, YL 3 years of experience in MR imaging) in assessing the N1 sign. Raters started their training to recognize the N1 territory by evaluating the 6 high resolution data sets and used these to draw a series of shapes for the SN based on the 0.67 mm, 1 mm and 1.34 mm thick slice data sets. Then, 80 HC cases were chosen randomly by one of the 4 raters to be age matched to the 80 Parkinsonism and related disorders cases. The renditions of the N1 sign were then fine-tuned as the raters went through the 80 age matched HCs. During this review, the characterization of the N1 appearance was refined in preparation for a blinded evaluation of the next 80 HC and 80 Parkinsonism and related disorders cases. One of the original four raters prepared the data independently for randomized viewing and the other three raters (ZC, NH and YL) then went through

the 4 to 5 most caudal slices of the SN and marked which type of feature was seen. In this group, only the tSWI data were reviewed unless there was an ambiguity that required the original magnitude, SWI or mIP SWI data. In those cases, all relevant images were reviewed. Raters were blinded as to whether the subject was Parkinsonism and related disorders or HC during this evaluation.

2.8. Evaluating the presence or absence of the N1 sign in HCs and Parkinsonism and related disorders patients

The first four to five caudal slices containing the SN were used to recognize the presence or absence of the N1 sign for all subjects. Bilateral loss of the N1 sign (BLN1) and unilateral loss of the N1 sign (ULN1) were defined as total loss of N1 in any of these first 5 slices bilaterally and unilaterally, respectively. The bilateral N1 sign (BN1) was defined as the bilateral presence of N1 in at least one slice. All Parkinsonism and related disorders patients were classified into three subgroups according to the N1 sign being BLN1, ULN1 or BN1. The global and local high iron content region (RII) (Liu et al., 2016) (pixel values above the 95% of the total susceptibility mean) susceptibilities of the SN were calculated using SPIN software (SpinTech, Inc., Bingham Farms, MI, USA) based on manually-drawn (by two of the authors and reviewed and corrected by a third senior author if necessary) deep gray matter structures on iSWIM (QSM) images with TE = 11 ms.

2.9. Statistical analysis

The inter-rater agreement was tested by Cronbach α statistics and the $p < 0.05$ was considered to be consistent statistically. The diagnostic test of loss of N1 sign between HCs and Parkinsonism and related disorders groups was carried out by a 2-sided Chi-square test or Chi-square test with Yates' correction (wherever there was a frequency under 5 in the square). The mean global and RII susceptibility comparisons between HCs and the Parkinsonism and related disorders subgroups were tested using a 2-tailed independent sample *t*-test. A $p < 0.05$ was set as statistical significance for all the tests. Statistical analysis was performed using SPSS (version 25.0; SPSS, Chicago, IL, USA).

3. Results

All 80 Parkinsonism and related disorders cases (IPD: 57; APs: 14; ET: 9; age: 63.8 ± 8.6 years; 43 males and 37 females) and 166/170 HCs (age: 63.6 ± 6.1 years; 62 males and 104 females) were finally enrolled for further analysis. Four HCs were excluded due to severe motion artifacts.

3.1. Results for preliminary analysis of 10 HC cases

Of the four cases evaluated for different FAs, the measured SNR was 26.5:1 ± 6.5 for 6° and 48.0 ± 12.6 for 9°. This gives a ratio of 1.8 ± 0.33 which is in line with the expected maximum increase in SNR of 1.5 (since for low FAs the signal behaves almost linearly with FA). In all subsequent scans, a 9° FA was used. Of the six cases evaluated for TH variation, the 1.34 mm thick slice provides the best SNR and largest coverage while still allowing for visualization of the N1 sign (Fig. 1). Basically, the SNR behavior relative to these GRE data acquisitions follows theoretical expectations.

Echo times on the order of 20 ms often showed the N1 sign when there was high iron in the SN, but roughly one-third of the time the magnitude images could not visualize the N1 sign. Much longer echo times showed larger blooming artifacts from the anterior high iron content in the SN as well as severe aliasing in this region from the air/tissue field inhomogeneities making the data less reliable. Also, as echo times increased, there was a degradation of image quality around the midbrain caused by the dephasing effects from the air/tissue frontal sinus interfaces and local susceptibility effects from the veins and the circle of Willis. The reviewers rated the 20 ms echo time as the best for visualization of the N1 sign with the least artifacts. (When these effects were severe enough to cause loss of signal in the midbrain area, the tSWI data from the TE = 11 ms was used in reviewing the data.) Fig. 2 shows an example of the ability to view the N1 sign with the different imaging types of magnitude, QSM and tSWI data with a TH of 0.67 mm, 1 mm and 1.34 mm and a TE of 20 ms. The use of mIP images is also shown to help visualize the N1 sign.

When the in-plane resolution and number of slices remains invariant, the different THs used are expected to have an SNR that is reduced according to the ratio of TH/THo where TH is the thickness of a given sequence and THo is the thickness of the reference scan. Therefore, we expect the 1 mm thick slice data to have an SNR of 3/4 of the 1.34 m data and the 0.67 mm thick slice data to have an SNR of 1/2 of the 1.34 mm data. The actual SNR is hard to measure directly from the image because of the spatial variation due to structural variability. The best two places found were the vitreous humor in the eye when there was no motion of the eye (3 cases) and in the muscle just below the eye at the edge of the brain (3 cases). The means/standard deviations of the SNR over the 6 cases for the 1.34 mm, 1 mm and 0.67 mm thick slices were 46.5 ± 3.0:1, 29.7 ± 2.4:1 and 21.7 ± 3.4:1, respectively, the latter two being in line with expectations.

In about one third of the cases, there was no evidence in the original T2*WI of any N1 sign even for an echo time of 20 ms. The issue, however, is not SNR or variability of the signal but rather CNR. In these cases, the susceptibility of the iron around the N1 region could be as low as 50 ppb, which was not enough to change T2* to visualize the N1 sign in the SN because there was little loss in signal in the T2*WI data. However, it was enough to be seen in the QSM data even though the CNR was not much more than 3:1. When the CNR was 5:1 or greater, then the N1 sign was easily visualized. The latter comments are equally true for both the QSM data and the tSWI data.

3.2. Results for the preliminary study of 76/80 HC training cases

3.2.1. Rater reliability and normal N1 sign variants

There was good consistency in reviewing the N1 sign among the 3 raters both in PD cases (left/right N1: Cronbach's α = 0.82/0.82; both $p<0.05$) and HCs (left/right N1: Cronbach's α = 0.73/0.83; both $p<0.05$). After reviewing the initial 76 HC cases, it was observed that the N1 sign manifested as different shapes from caudal to cranial slices. These N1 sign characteristics included: one tail (leg or projection, Fig. 3A, B), STS (Fig. 3C, D), incomplete loop (Fig. 3E), complete loop (Fig. 3F, G, H) and a cluster arrangement (Fig. 3I, J). All these are potentially representative of a normal N1 sign. Table 1 shows the number of unique HCs where N1 manifested as STS, loop, or a combination of both, for each side. We found that 74/76 and 73/76 cases showed the N1 as either a loop or STS sign in the right and left SN, respectively (see Table 2 for cases with bilateral loop sign, bilateral STS, and loop + STS). These results show that not only is the loop sign more likely to be seen compared to the STS, but that it's seen over more slices compared to the STS.

3.2.2. Several special features of the N1 sign

1) The signal from the N1 region appears bright inside the loop or STS but this is sometimes an optical illusion as the signal inside is, in fact, often the same as the surrounding signal outside the SN. However, on occasion, the signal inside was actually brighter than the surrounding hyperintense tissue. 2) When there was just one tail visible on a given slice, a minimum intensity projection (mIP) over two adjacent slices was found to reveal N1 more clearly than the individual images (Fig. 2). This is because individual tails were seen on the thin slices used. However, usually an adjacent slice shows the loop sign. There were only two cases where no loop sign was present and the two single tail signs showed in adjacent slices. 3) When viewing mIPs of the SN in the middle slices, N1 shows more often as a loop rather than the STS in

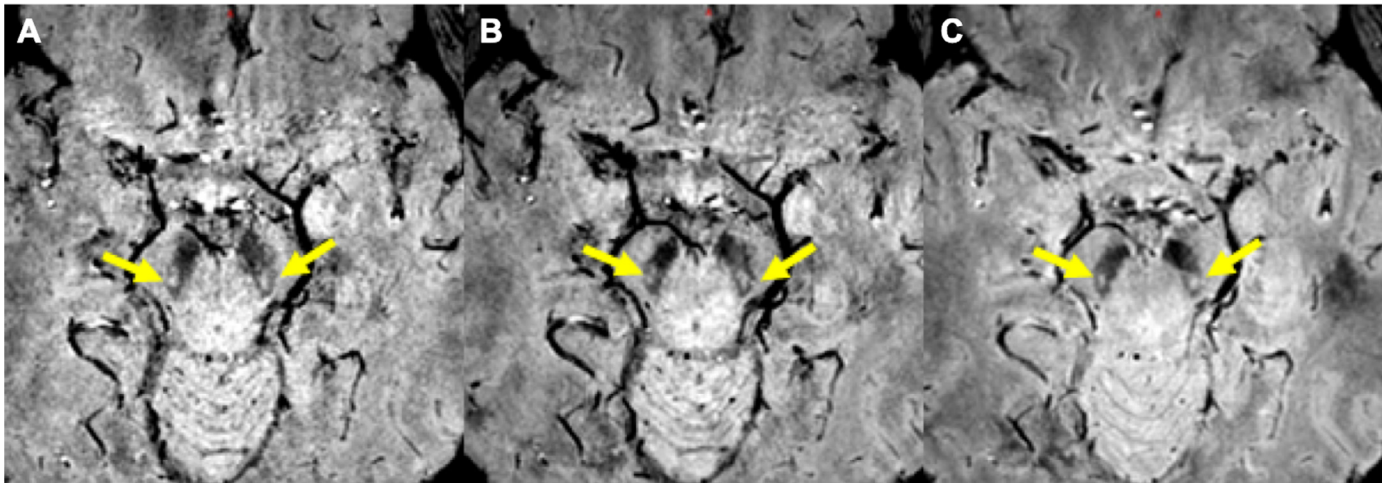

Fig. 1. A comparison of N1 manifestation (yellow arrows) from three different scans with THs: A) 0.67 mm, B) 1 mm and C) 1.34 mm. The in-plane resolution is 0.67 mm x 0.67 mm for each acquisition, the number of slices is 96 and the total acquisition time is the same for each scan.

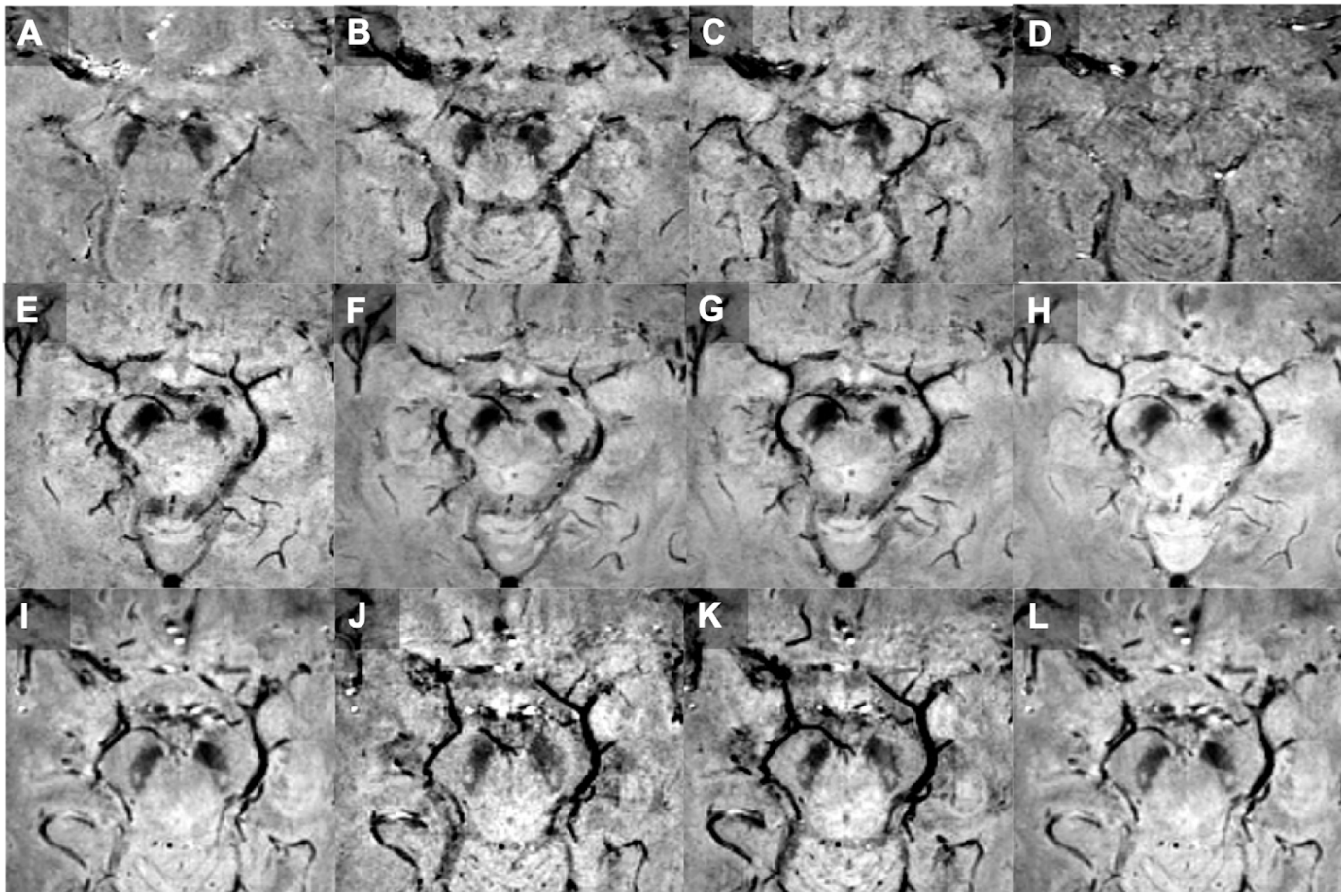

Fig. 2. All of the images above have a resolution of 0.67 mm x 0.67 mm in plane and a TH of 1.34 mm unless otherwise noted. Here, mIPn means a minimum intensity over n adjacent slices. First row: A) QSM; B) tSWI mIP3; C) tSWI mIP3, adjacent slice; and D) T2*WI. Second row, E) tSWI, TH = 0.67 mm, mIP4; F) tSWI, TH = 1 mm, mIP3; G) tSWI, TH = 1 mm, mIP3, adjacent slice; and H) tSWI, TH = 1.34 mm, mIP2. Third row: I) tSWI; J) tSWI with TH = 0.67 mIP2; K) magnitude with TH = 1 mm mIP2; and L) a repeat of the image in I) for visualization purposes.

which the bright N1 is surrounded by dark signal from the rest of the SN structure. 4) Only two cases showed the STS in the original magnitude images where it had not been seen previously in the tSWI data but these two also had loop signs in adjacent slices, so this feature did not change the sensitivity or specificity of the review. 5) The appearance of the STS can occur in the original magnitude image even when the iron content in the QSM images does not show the same effect (two cases seen in the PD data). This "fake" STS can be caused by T2* dephasing at the edge of the high iron content in the SN (Fig. 4). And 6) the 0.67 mm x 0.67 mm x 1.34 mm data can be interpolated to 0.67 mm isotropic to create reasonably good 3D reformatted images (Fig. 5). In this multi-planar reformatted view, the caudal portion of the SN can be seen to be almost

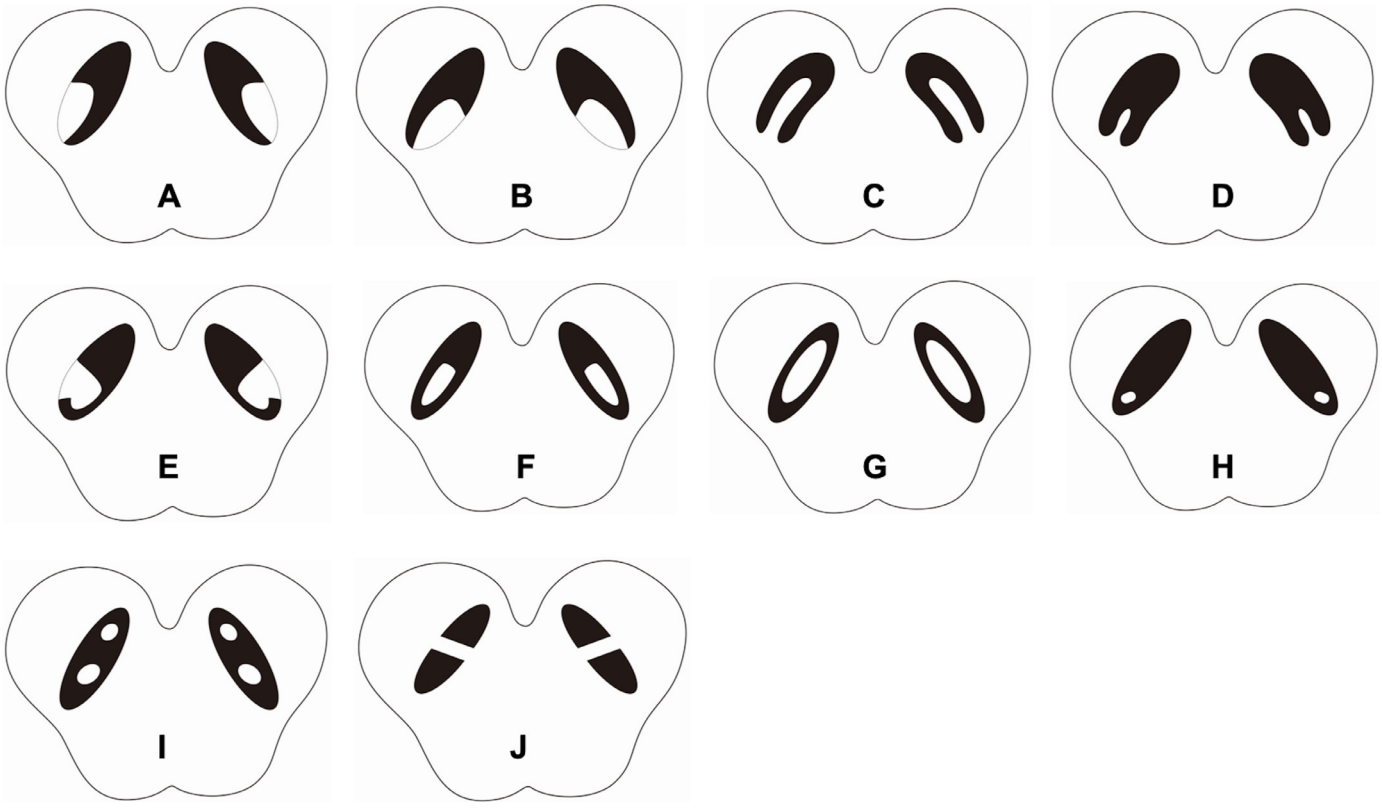

Fig. 3. Cartoon illustration of the nigrosome 1 variants. A-D in the first row show the swallowtail sign variants due to the scanning plane or individual iron content in the normal nigrosome 1; E-H in the second row show the loop or ovoid sign variants; and I-J in the third row show the nigrosome 1 as a cluster or strip sign.

Table 1
Number of people showing the nigrosome 1 (N1) sign as a function of slice number. Here, Σ = cumulative number of N1 signs in consecutive slices (1–5; from caudal to cranial); HC = healthy control; STS = swallowtail sign; *R* = right side; *L* = left side; STS + Loop = either STS or loop sign served as the N1 sign; STS_bi = bilateral STS; Loop_bi = bilateral loop sign; STS-Loop = STS on one side and loop on the other side as marker of the N1 sign.

Slice N1\sign (number)	1	2	3	4	5
∑HC − STS	4	14	43	56	59
R	3	8	27	33	33
L	1	6	16	23	26
∑HC − Loop	29	84	118	136	140
R	21	49	61	70	72
L	8	35	57	66	68
∑HC − STS + Loop	33	93	133	146	147
R	24	53	71	74	74
L	9	40	62	72	73
∑HC − STS_bi	0	0	7	11	12
∑HC − Loop_bi	5	23	42	51	52
∑HC − STS − Loop	1	7	17	20	25

Table 2
Occurrence of loop sign versus swallowtail sign (STS) as a function of slice number for the training set of 76 cases. $Loop_{bi}$ = bilateral loop sign; STS_{bi} = bilateral swallowtail sign; Loop + STS = loop sign on one side and STS on the other side. Usually the N1 sign appears in the 2nd, 3rd and 4th slices but much of this depends on the partial volume effect whether it is seen on the 1st or 5th slice as well.

Slice\N1sign (number)	1	2	3	4	5
$Loop_{bi}$	5	22	28	25	6
STS_{bi}	0	0	7	4	1
Loop + STS	1	7	11	3	5
sum	6	29	46	32	12

in-plane to the pseudo transverse acquisition (the data were collected along the AC-PC line) and so the loop sign shows very well in this case. This is not always the case, however, and depends on the shape of the SN for each individual.

3.3. Results of evaluating the N1 sign for the blinded study of 80 HCs and 80 Parkinsonism and related disorders patients

Of the second set of 80 HCs used in this blinded study, 97% (78/80) showed either a clear loop or STS in at least 2 slices, including 5 unilaterally and 73 bilaterally. The other 2 HCs showed total loss of N1 sign, bilaterally. There were 69 HCs that showed a bilateral loop sign (86%), 4 HCs (5%) showed a unilateral loop sign along with unilateral STS and 5 showed a unilateral loop sign. For the PD and APs data, 54% (38/71) (32 IPD and 6 APs) did not show either a loop or STS-like N1 sign bilaterally, 25%%(18/71) (12 IPD and 6 APs) showed either a loop (11 IPD and 5 APs) or STS (1 IPD and 1 APs) unilaterally, and the remaining 21% (15/71) (13 IPD and 2 APs) showed bilateral loop signs (11 IPD and 2 APs) or a unilateral loop sign along with a unilateral STS sign (2 IPD) (see Table 3). The sensitivity and specificity of loss of N1 sign (BLN1 and ULN1) using tSWI in differentiating HC from IPD/APs was 85%/86% and 91%/86%, respectively, and the overall sensitivity and specificity in differentiating HC from IPD and APs was 91% and 79%, respectively. The 9 ET cases contained the normal loop sign or STS on at least 1 slice bilaterally. An example set of slices covering the entire SN and STN are shown in Fig. 6 for a HC and in Fig. 7 for an IPD patient. For image viewing to assess the presence or absence of the N1 sign, QSM and tSWI data were used from the second echo in 59 cases and from the first echo in 23 cases (due to some aspects of the SN being lost due to large local field effects by the surrounding air/tissue and teeth interfaces).

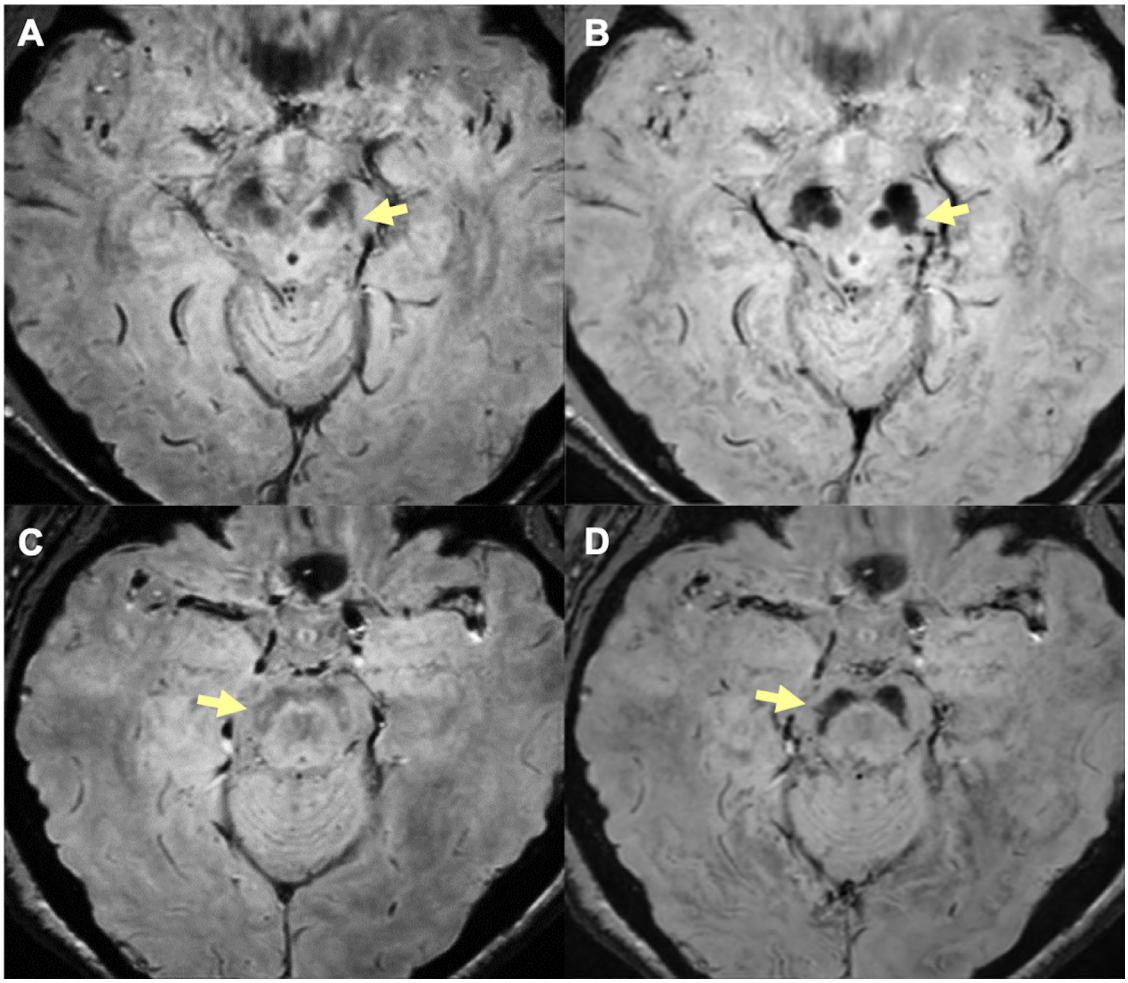

Fig. 4. High iron content can lead to T2* dephasing at the edge of the SN. Magnitude images show the "putative STS" (A, yellow arrow) and the "loop" sign (C, yellow arrow) while tSWI images show the SN without any indication of a STS (B, D), edges of the SN shown with the yellow arrow). This fake STS is an artifact of T2* dephasing at the edge of an object with high iron content. These 2 different IPD cases (A and B; C and D) have the same standard imaging parameters.

3.4. Susceptibility quantification in SN

There were 80 HC, 57 IPD, 14 APs and 9 ET cases included in the iron analysis. All iron analysis presented herein was done with the QSM data from the first echo. (When comparing whole region susceptibility for TE 11 vs TE 20, the R-squared for the linear fit for all midbrain and basal ganglia structures was 0.87 and 0.86 for the right and left side of the brain, respectively.) Both the mean global and RII susceptibility of the right and left side of the SN in IPD (BLN1), APs (BLN1) and APs (ULN1) were higher than those of HC (BN1). While the mean values in IPD (ULN1), IPD (BN1) and ET (BN1) did not differ significantly from those in HC (BN1) (see **Table 4** for the statistical analysis results).

4. Discussion

The key findings in this paper relate to creating a robust high quality, rapid imaging protocol for clinical use in detecting the loss of the N1 sign in PD patients, characterizing the shape of the N1 in the SN, and comparing iron content with the presence or absence of the N1 sign as a biomarker to distinguish PD from HC. Specifically, sufficient in-plane resolution, TH and SNR are required to best image the SN. In this work, we found that a resolution of 0.67 mm x 0.67 mm x 1.34 mm met these criteria providing a practical means to image most of the brain from below the level of the dentate nucleus to the top of the brain. The choice of 9° for the flip angle kept the signal high and at the same time minimized ghosting artifacts from pulsatile flow from the arteries. From the 80 HC and 80 Parkinsonism and related disorders cases blindly reviewed, we found that a high prevalence of HCs (97.5%, 78/80) and ET (100%, 9/9) showed the N1 sign, whereas only 15 out of 71 IPD/APs showed the N1 sign. Those IPD/APs patients with bilateral loss of the N1 sign showed the highest iron content in the SN relative to all other groups.

4.1. Evaluating the N1 sign

Since the amount of iron in the SN varies in each individual, the original magnitude images did not always reveal a clear delineation of the SN or the N1 sign. The use of QSM overcame this difficulty providing a clear delineation of the iron in the SN. However, to visualize the N1 more clearly, and keep information from the background tissue, we also used tSWI as a means to review the data. Since the air/tissue interface from the nasal region can severely affect the quality of the QSM data in this region, when necessary, we used the TE 11 ms data to create the susceptibility maps. The resulting susceptibility is independent of echo time (although the SNR of the susceptibility maps does depend on echo time).

The N1 territory can appear in many shapes depending on the orientation of the imaging plane. These shapes are outlined in **Fig. 3** manifesting as either a complete or incomplete loop, an STS with short or long legs, and even a cluster or a strip. The cluster and strip sign were noticed in the most inferior 2 slices of 16/76 HCs, which might due to the individual difference of N1 or mingling with other nigrosomes such

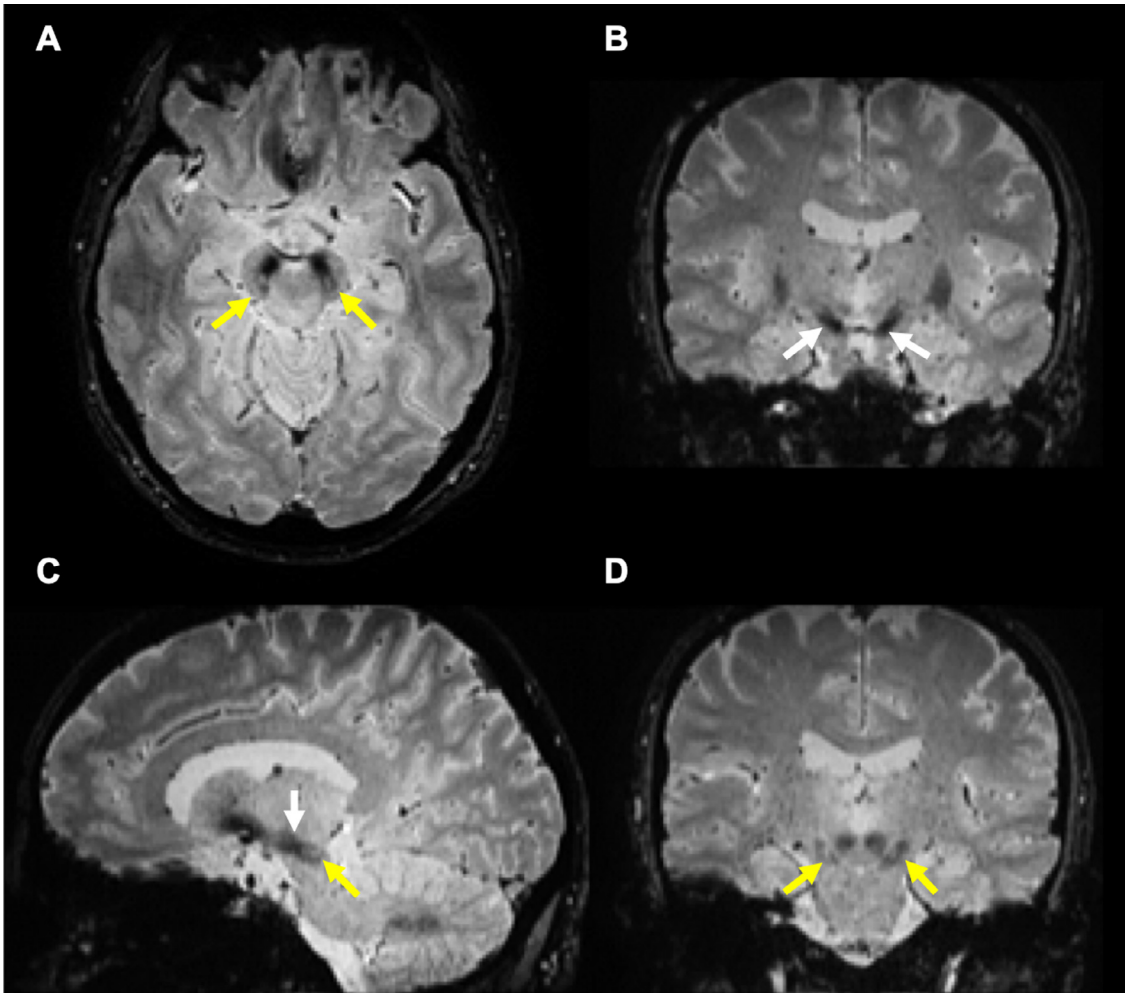

Fig. 5. 3D reformatting of 1.34 mm data after interpolation into 0.67 mm isotropic data. Image (A), an example slice showing the N1 sign (yellow arrows) in the original data collected in the transverse plane; image (B), a reformatted coronal image showing the SN (white arrows); image (C) a reformatted sagittal image showing the SN and N1 sign; and image (D) a reformatted coronal image showing the N1 sign.

Table 3
Analysis of the 80 HC and 80 Parkinsonism and related disorders cases for the SN loop and STS. Here, 78 HC cases showed clear loop/STS bilaterally. All 9 ET cases showed a normal loop/STS. For the IPD/APs/ET data, 38 showed bilateral loss of loop/STS sign, 18 with unilateral loss of loop/STS sign and the other 15 appeared normal with either the loop or STS sign, bilaterally. ET = essential tremor (ET); APs = atypical Parkinsonian syndromes (e.g. multiple system atrophy, progressive supranuclear palsy); IPD = idiopathic Parkinson's disease; HC = healthy control.

Cohort\ groups	ET	APs	IPD	HC
bilateral loss of N1	0	6	32	1
unilateral loss of N1	0	6	12	1
bilateral N1	9	2	13	78
sum	9	14	57	80

as N3 and N4, especially the cluster sign. However, it should be noted that with high resolution, the N1 sign appears mostly as a loop and on occasion as an STS. Sometimes, the N1 sign could still be considered as present even if there is just a single tail medially at the caudal edge of the SN with an adjacent slice showing a single leg on the lateral side. Taking the mIP of over several slices will still show the N1 sign (Fig. 2E-H). So, one has to consider that the tissue adjacent to these two legs is also part of the N1. It should be noted that taking the mIP over two slices is not the same as having collected the data with a slice that is two times thicker than the original data. It keeps the information intact without partial volume effects inherent in thicker slices. In most other cases, the N1 sign shows in the second, third and fourth slices (likely because the first slice often had only a tip of the SN in it and was significantly partial volumed). Generally, we recommend that the following four images should all be reviewed when making an assessment as to the presence or absence of the N1 sign: the original magnitude images, the SWI data, the QSM data and the tSWI data. On occasion, we found that the QSM data was blurred and it became difficult to assess the presence of the N1 sign. Also, we found in nearly one third of the cases with low iron in the N1 region little to no evidence of the SN could be seen in the magnitude images but could be seen easily using the QSM or tSWI data (Kim et al., 2018).

4.2. The role of tSWI in visualizing the N1 sign

The high SNR (46.5:1) in the magnitude image leads to a susceptibility error of between 10 and 15 ppb. Given a low iron content in the SN and a susceptibility of only 50 ppb (a CNR of roughly 3:1), it is difficult to distinguish the N1 sign. However, if there are say $N = 25$ pixels in the N1 territory, then the Rose criteria dictates that the effective visibility increases to CNR*sqrt(N) = 15:1 and the general shape of the N1 sign can be seen clearly in the QSM data. When the iron content is low which is often the case for younger people the R2* effect will be low and, therefore, the N1 sign may not be visible. The advantage of tSWI is that it marries both the magnitude and QSM data so

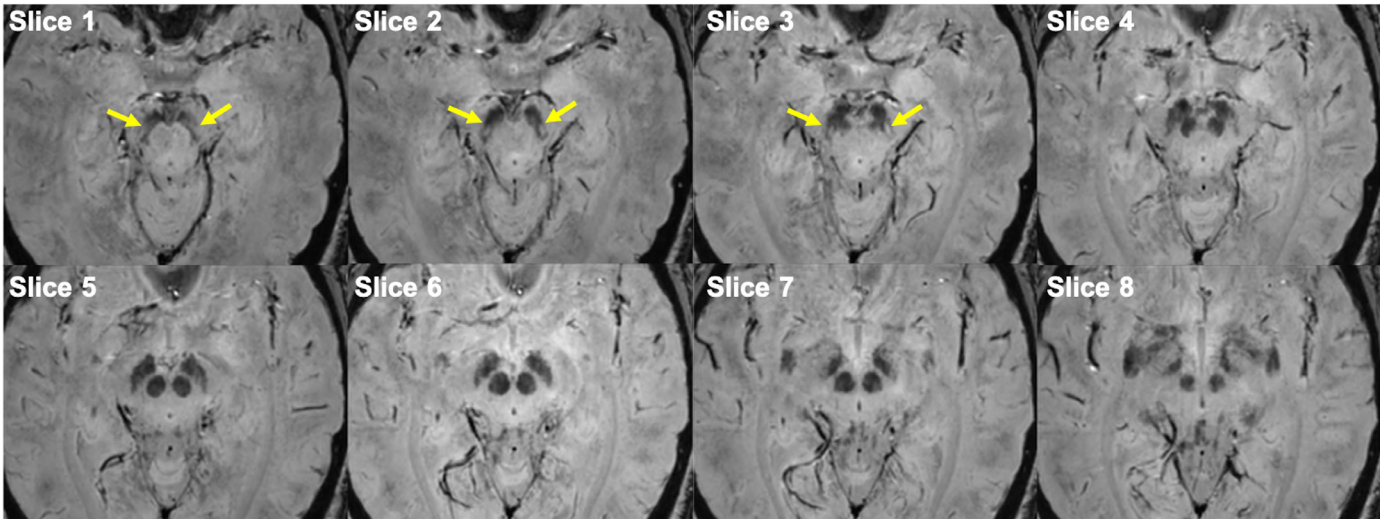

Fig. 6. Consecutive slices through the SN and STN for a healthy control (70 years old male). Notice of the normal N1 variants on tSWI: incomplete loop sign (slice 1-yellow arrow, type E in Fig. 3), complete loop sign (slice 2–3-yellow arrow, type F in Fig. 3).

that even if the N1 sign is not visible in the magnitude image it will be visible in the tSWI data thanks to the contrast in the QSM data. For older people, the susceptibility (putative iron content) is much higher (usually on the order 100 ppb) and it is easier to see the N1 sign on both the magnitude and QSM data as well as the tSWI data.

4.3. Previous work on the role of the presence of N1 in PD patients

Several works have evaluated the N1 sign with high resolution at 7T (Blazejewska et al., 2013; Gramsch et al., 2017; Kim et al., 2016; Lee et al., 2016; Schmidt et al., 2017). Blazejewska et al. (Blazejewska et al., 2013) discuss the potential to visualize the N1 territory at 7T as a hyperintense, ovoid area (a loop) within the dorsolateral border of the otherwise hypointense SNpc. Only a small number of in vivo and postmortem HCs (8 and 2, respectively) and PD cases (10 and 1, respectively) were studied using T2*-weighted 3D GRE. Of 10 PD patients, there was a bilateral absence of the N1 and for the 8 HCs, there was a bilateral presence in 7 cases (Blazejewska et al., 2013). They suggest that the absence of the N1 sign in PD could be due to: neuronal cell loss, neuromelanin loss, an increase in iron content in N1, a change in iron oxidation or a combination of these effects. Whether or not an increase in iron content is simply a biomarker of neuromelanin depigmentation or a partial cause of the loss of neuromelanin remains unknown. Gramsch et al. (Gramsch et al., 2017) investigated 46 HC (19 to 75 y) using SWI at 7T. The overall specificity of N1 was quoted as 94% (43/46 could be classified as normal: N1 was clearly visible bilaterally or unilaterally). There was no correlation of N1 visibility with age. Kim et al. (Kim et al., 2016) showed a loss of N1 in 30 of 30 PD cases and the presence of the N1 sign in 26 of 26 HC in their 7T study. Alterations of the nigral hyperintensity, both partial and complete loss, were found on the unaffected side in patients with hemi-parkinsonism and were confirmed by ^{123}I-FP-CIT-SPECT. In certain elderly subjects, nigral hypointensity appeared to be more prominent than in others, suggesting a possible confounding effect as the patient ages and iron naturally accumulates with age. This phenomenon may be consistent with the increase in the concentration of neuromelanin-iron complex

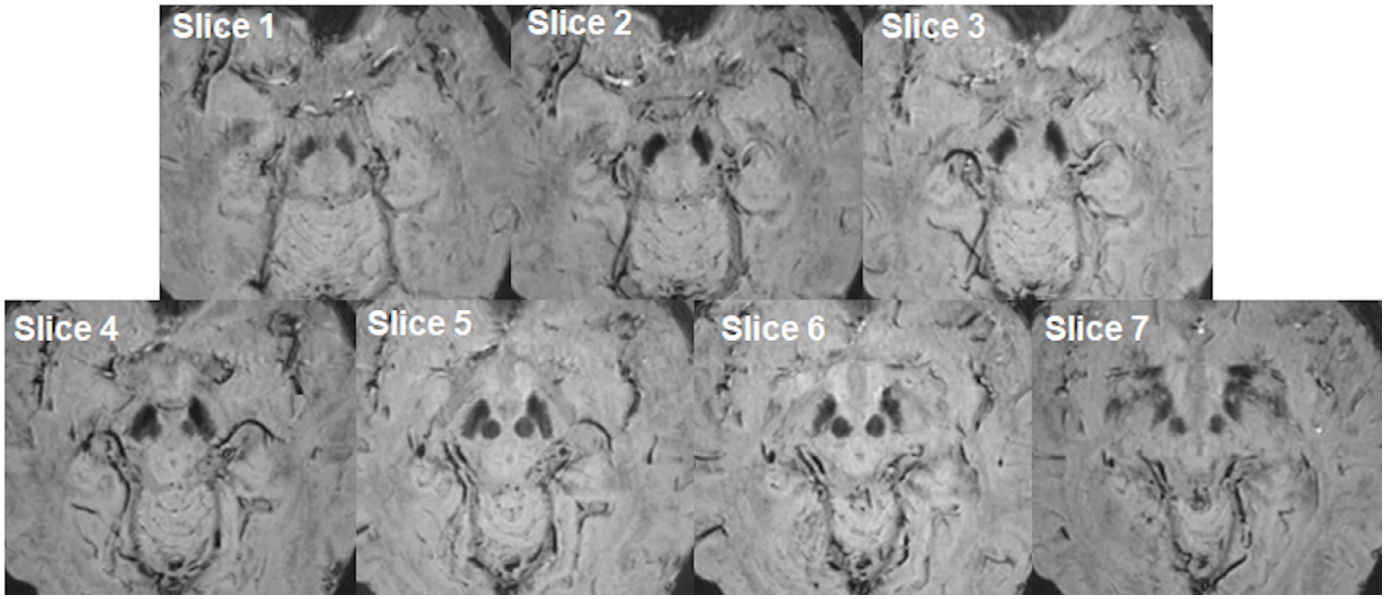

Fig. 7. Consecutive slices going from inferior to superior levels through the SN and STN for an idiopathic Parkinson's Disease patient (78 years old male, involuntary tremulous motion of bilateral upper limbs for 4 years, MMSE = 29, UPDRS-III = 32, H&Y = 2). Notice the bilateral loss of the N1 sign on tSWI.

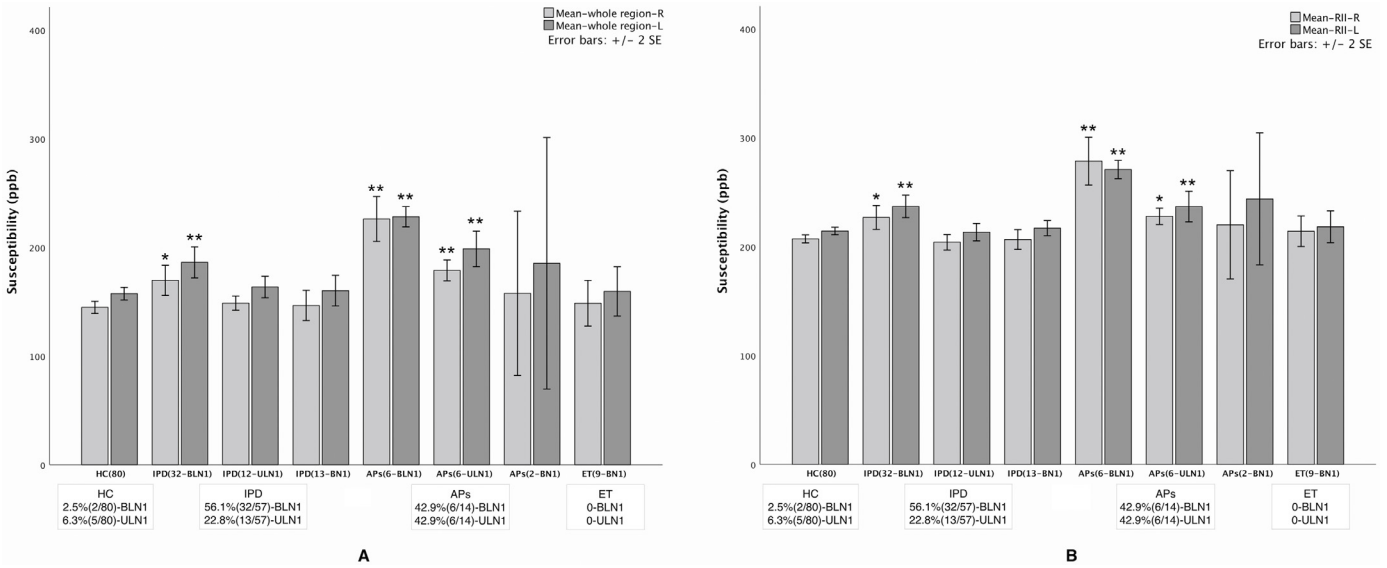

Fig. 8. Mean measures for both the global (A) and RII (B) iron analysis along with the N1 loss for all groups. The IPD/APs with bilateral loss of the N1 sign (BLN1) and APs with unilateral loss of N1 (ULN1) showed significantly higher mean iron content than the HCs (* $p < 0.05$; ** $p < 0.001$). The number of cases and percentage of N1 loss in each sub-group is listed under the corresponding bar, respectively; IPD = idiopathic Parkinson's Disease; APs = atypical Parkinsonian syndromes; ET = essential tremor; BLN1 = bilateral loss of N1; ULN1 = unilateral loss of N1; and BN1 = bilateral presence of N1.

Table 4
Statistical analysis of global and RII susceptibility of SN between HC, IPD, APs and ET. Numbers in bold indicates statistical difference. IPD = idiopathic Parkinson's Disease; APs = atypical Parkinsonian syndromes; ET = essential tremor; BLN1 = bilateral loss of N1; ULN1 = unilateral loss of N1; and BN1 = bilateral presence of N1.

subgroups	mean susceptibility of SN (ppb, mean ± sd)			
	global		RII	
	right	left	right	left
HC	145 ± 25	157 ± 25	207 ± 16	214 ± 15
IPD (BLN1)	170 ± 39	186 ± 40	227 ± 31	237 ± 29
IPD (ULN1)	149 ± 11	164 ± 17	204 ± 12	213 ± 14
IPD (BN1)	147 ± 25	160 ± 25	206 ± 16	217 ± 13
APs (BLN1)	226 ± 25	228 ± 11	278 ± 27	271 ± 10
APs (ULN1)	179 ± 11	199 ± 20	228 ± 9	237 ± 17
APs (BN1)	158 ± 53	185 ± 82	220 ± 35	244 ± 43
ET (BN1)	149 ± 32	160 ± 34	214 ± 21	218 ± 22
	p			
HC vs. IPD (BLN1)	**0.002**	**0.001**	**0.002**	**<0.001**
HC vs. IPD (ULN1)	0.380	0.423	0.535	0.822
HC vs. IPD (BN1)	0.812	0.715	0.905	0.560
HC vs. APs (BLN1)	**<0.001**	**<0.001**	**<0.001**	**<0.001**
HC vs. APs (ULN1)	**0.001**	**<0.001**	**0.003**	**0.001**
HC vs. APs (BN1)	0.482	0.713	0.279	0.508
HC vs. ET (BN1)	0.678	0.819	0.235	0.492

with age in SN (Pavese and Tai, 2018).

Still, the typical N1 sign is not always visible even in the HCs on ultra-high field SWI (Schmidt et al., 2017) in which study they collected oblique-axial images-perpendicular to the long axis of the midbrain with a resolution of 0.8 mm isotropic. The reason might be the individually variable microstructural organization of N1, just as a recent investigation reported that metal-bound, intra- and extracellular neuromelanin macromolecules might cause a hypointense signal of N1 in T2*/SWI imaging, especially at high magnetic field strengths (Lee et al., 2016). Finally, another high field work using high resolution SWI at 7T showed the N1 sign in 9 healthy controls and all the veins associated with the midbrain region. They noted that in all 5 cadaver brains studied that the microvessels ran through the dorsal pars compacta and along the caudolateral circumference of the red nucleus. Many vessels also cut across the SN and the cerebral peduncle. On occasion, some of these vessels may have obscured the visualization of the N1 sign or caused a swallowtail mimic (Kau et al., 2019). Their resolution was 0.23 mm x 0.23 mm x 0.62 mm making it possible to see the small veins. In this paper, we used 0.67 mm x 0.67 mm x 1.34 mm which is roughly 36 times lower resolution. Therefore, these veins were not generally visible in our images and we saw no specific case indicative of a vein confounding the interpretation of the N1 sign.

A number of papers have investigated the different nigrosome territories. Although 9.4T cadaver brain work has shown the nigrosome structures very well (Massey et al., 2017), it has been noted that segmenting N1 to N5, especially, N2 to N5 in PD, can be challenging even at 7T (Schwarz et al., 2018). Isolating the various nigrosome components may be important too, although it has been shown that N1 is most prominently affected in the early stage of the disease followed by N2-N5 and then the iron-rich SN pars reticulata in later stages of the disease (Damier et al., 1999b). One group (Nam et al., 2017) used a form of tSWI (referred to as SMWI). They did some ground-breaking work in this area using high resolution imaging (0.5 mm x 0.5 mm x 1 mm) to show the improved sensitivity with this method (in agreement with our findings). This same group (Sung et al., 2018) then used this approach to study 128 IPD patients (early stage: $n = 89$; late stage: $n = 39$) and 15 HCs. They showed that the loss of the hyperintensity was more often in N1 (65.2%) in early stage IPD (178 SNs) but in both N1 and N4 (34.8%) in late stage PD where the loss in only the N1 (25.6%) was less prevalent than that in both N1 and N4 (74.4%). Nevertheless, intact SNs (both N1 and N4) were found in 17 SNs of the early stage IPD (9.6%), while, it was not found in any SNs of the late stage IPDs. In addition, involvement of both N1 and N4 on both sides was found in 19.1% of the early stage IPDs, whereas it was higher (61.5%) in the late stage IPDs.

Generally, the sensitivity and specificity of using the N1 sign have been found to be above 80%. Bae et al. (Bae et al., 2016) investigated whether 3T SWI could accurately detect the alterations of N1 in PD, MSA and PSP, and using ^{123}I-FP-CIT SPECT, they found that the sensitivity and specificity of SWI were 88.8% and 83.6%, respectively (126 PD, 11 MSA,11 PSP, 26 HCs, 36 disease controls). Sixteen cases with parkinsonism showed intact N1 bilaterally (false-negative), and this finding did not correlate with age or symptom duration. Eleven cases were false-positive, and there was no apparent explanation. In addition, the specificity was a little bit lower than that of previous reports, which

the authors ascribed to the lower resolution used in their study (0.63 mm × 0.63 mm × 2 mm). In our study, the sensitivity and specificity of the N1 sign using tSWI in differentiating HC from IPD and PDS was 85%/86% and 91%/86%, respectively, which is similar to the results in these other papers. Two meta-analyses based on Pubmed papers from 2005 to 2017 found that using the N1 sign had a high sensitivity and specificity (94.6%/94.4% at 3T; 97.7%/94.6% at 3T + 7T) in distinguishing PD from healthy controls (Mahlknecht et al., 2017; Pavese and Tai, 2018), though it is unable to reliably separate PD from atypical Parkinsonism. Reduced NM-related signals and/or volume loss in NM containing structures have been found in PD patients. Pavese et al. (Pavese and Tai, 2018) suggest that longitudinal changes of NM signal can be detected in PD, raising the possibility of using it as a marker of disease progression. Mahlknecht (Mahlknecht et al., 2017) notes that in two of these studies, the absence of dorsolateral nigral hyperintensity predicted ipsilateral dopamine-transporter deficiency with 87.5% sensitivity and 83.6% specificity.

4.4. The relationship between bilateral N1 loss and iron content

One of our major findings is the increased iron content of the SN for patients with bilateral loss of N1. We found that there was a significant difference between patients with a bilateral loss of N1 and HCs of about 30 ppb. A recent paper also found significantly higher iron in the SN of PD patients compared to HC by roughly 25 ppb (Kim et al., 2018). In our work, susceptibilities for the whole SN of HC ranged from 130 to 170 ppb with an average around 150 ppb. This is much higher than the numbers quoted in their work which were closer to 100 ppb. The reason for the smaller increase may be because their QSM reconstruction method gave lower susceptibilities than our approach. From a percentage perspective, both groups found a difference of roughly 20% between PD patients and HC. The increase in iron content is likely due to the filling of the N1 territory with iron after it depigments. However, increases in other parts of the SN cannot be ruled out. Historically, there have been more than 30 years of publications suggesting that MRI can find higher levels of iron in some PD patients but not all of them. Our finding that the patients with bilateral loss of the N1 sign have the highest iron content helps to sub-characterize the patient groups. Most of the patients who have high iron content are from this group with-bilaterlal loss of the N1 sign (18 out of 24 IPD and APs with iron content of more than 162 ppb). If these are used as an independent group, then this clearly explains why some PD patients show significant increases in iron content while others do not.

4.5. Limitations of this work

First, we set the longest echo time to be 20 ms so the magnitude image will have limited signal loss for low iron content (although this was ameliorated by using tSWI). Second, we did not measure the volume of the N1 specifically which could be used to predict potential increases in iron content after the neuromelanin in the N1 territory depigments. Third, each individual has a unique orientation of the SN and finding the N1 sign would be best done either along the long axis of the caudal part of the SN or perpendicular to it. The former would lead to an elongated loop and the latter to smaller cross-sectional circles. To do this perfectly would require two scans, one for each of the left and right SN. In this work, the resolution was high enough in-plane and through plane to view the different manifestations of the N1 sign despite these different orientations not being collected.

5. Conclusions

The nigrosome 1 territory (the N1 sign) can be consistently visualized with the following scanning parameters on SWI at 3T: acquisition along the AC-PC line, resolution of 0.67 mm x 0.67 mm x 1.34 mm, TE of 20 ms and FA of 9°. Interpreting the N1 sign can be difficult because it can take many forms but the high resolution data and a clear characterization of the N1 appearance helps to make that decision easier. We recommend using tSWI as the principal image to visualize the N1 sign followed by the original magnitude, SWI or mIP SWI image as supporting data. Further, the 4 to 5 caudal most slices of the SN should be reviewed to find the N1 sign. Most healthy controls show the N1 sign while many PD/APs patients do not. Those PD/APs patients with bilateral loss of the N1 sign showed the strongest increases in iron content.

Funding

This work was supported in part by a grant from the Science and Technology Commission of Shanghai Municipality (17411952700) for Fuhua Yan, M.D., Naying He, M.D., Zenghui Cheng,M.D., and Yan Li, M.S.; a grant from the Shanghai Sailing Program(18YF1414700) for Naying He, M.D., Yan Li, M.S. and the National Natural Science Foundation of China (grant number: 81971576 for Fuhua Yan, M.D., Naying He, M.D., Zenghui Cheng,M.D.; grant number: 81801652 for Naying He, M.D. and E. Mark Haacke, PhD; grant number: 81430022, 91332107, 81371407 for Shengdi Chen, M.D.; grant number: 81801267 for Pei Huang, M.D.).

Data availability statement

The MR imaging and clinical data used to support the findings of this study are will be available from the corresponding authors upon request after the entire data collection procedure and project are completed.

Declaration of Competing Interest

The authors declare that the research was conducted in the absence of any commercial or financial relationships that could be construed as a potential conflict of interest.

Acknowledgments

We sincerely acknowledge Cheng Ren (M.A., Hangzhou Yasheng Brand Design Co., Ltd.) for her assistance in drawing the cartoon illustration of the nigrosome 1 variants. We also thank all the participants in this study.

References

Bae, Y.J., Kim, J.M., Kim, E., Lee, K.M., Kang, S.Y., Park, H.S., Kim, K.J., Kim, Y.E., Oh, E.S., Yun, J.Y., Kim, J.S., Jeong, H.J., Jeon, B., Kim, S.E., 2016. Loss of Nigral hyperintensity on 3 Tesla MRI of Parkinsonism: Comparison with (123) I-FP-CIT SPECT. Mov. Disord. 31, 684–692. https://doi.org/10.1002/mds.26584.

Blazejewska, A.I., Schwarz, S.T., Pitiot, A., Stephenson, M.C., Lowe, J., Bajaj, N., Bowtell, R.W., Auer, D.P., Gowland, P.A., 2013. Visualization of nigrosome 1 and its loss in PD: pathoanatomical correlation and in vivo 7 T MRI. Neurology 81, 534–540. https://doi.org/10.1212/WNL.0b013e31829e6fd2.

Damier, P., Hirsch, E.C., Agid, Y., Graybiel, A.M., 1999a. The substantia nigra of the human brain. I. Nigrosomes and the nigral matrix, a compartmental organization based on calbindin D(28K) immunohistochemistry. Brain 122, 1421–1436 Pt 8.

Damier, P., Hirsch, E.C., Agid, Y., Graybiel, A.M., 1999b. The substantia nigra of the human brain. II. Patterns of loss of dopamine-containing neurons in Parkinson's disease. Brain 122, 1437–1448 Pt 8.

Deuschl, G., Bain, P., Brin, M., 1998. Consensus statement of the movement disorder society on tremor. Ad Hoc Scientific Committee. Mov. Disord. 13, 2–23 Suppl 3.

Du, G., Liu, T., Lewis, M.M., Kong, L., Wang, Y., Connor, J., Mailman, R.B., Huang, X., 2016. Quantitative susceptibility mapping of the midbrain in Parkinson's disease. Mov. Disord. 31, 317–324. https://doi.org/10.1002/mds.26417.

Gilman, S., Low, P.A., Quinn, N., Albanese, A., Ben-Shlomo, Y., Fowler, C.J., Kaufmann, H., Klockgether, T., Lang, A.E., Lantos, P.L., Litvan, I., Mathias, C.J., Oliver, E., Robertson, D., Schatz, I., Wenning, G.K., 1999. Consensus statement on the diagnosis of multiple system atrophy. J. Neurol. Sci. 163, 94–98.

Gramsch, C., Reuter, I., Kraff, O., Quick, H.H., Tanislav, C., Roessler, F., Deuschl, C., Forsting, M., Schlamann, M., 2017. Nigrosome 1 visibility at susceptibility weighted 7T MRI-a dependable diagnostic marker for Parkinson's disease or merely an inconsistent, age-dependent imaging finding? PLoS One 12, e0185489. https://doi.org/10.

1371/journal.pone.0185489.
He, N., Huang, P., Ling, H., Langley, J., Liu, C., Ding, B., Huang, J., Xu, H., Zhang, Y., Zhang, Z., Hu, X., Chen, S., Yan, F., 2017. Dentate nucleus iron deposition is a potential biomarker for tremor-dominant Parkinson's disease. NMR Biomed 3010.1002/nbm.3554.
He, N., Ling, H., Ding, B., Huang, J., Zhang, Y., Zhang, Z., Liu, C., Chen, K., Yan, F., 2015. Region-specific disturbed iron distribution in early idiopathic Parkinson's disease measured by quantitative susceptibility mapping. Hum. Brain Mapp. 36, 4407–4420. https://doi.org/10.1002/hbm.22928.
Hoehn, M.M., Yahr, M.D., 1967. Parkinsonism: onset, progression and mortality. Neurology 17, 427–442.
Kau, T., Hametner, S., Endmayr, V., Deistung, A., Prihoda, M., Haimburger, E., Menard, C., Haider, T., Hoftberger, R., Robinson, S., Reichenbach, J.R., Lassmann, H., Traxler, H., Trattnig, S., Grabner, G., 2019. Microvessels may confound the "Swallow tail sign" in normal aged midbrains: a postmortem 7 t sw-mri study. J. Neuroimaging 29, 65–69. https://doi.org/10.1111/jon.12576.
Kim, E.Y., Sung, Y.H., Shin, H.G., Noh, Y., Nam, Y., Lee, J., 2018. Diagnosis of early-stage idiopathic parkinson's disease using high-resolution quantitative susceptibility mapping combined with histogram analysis in the substantia nigra at 3 T. J. Clin. Neurol. 14, 90–97. https://doi.org/10.3988/jcn.2018.14.1.90.
Kim, J.M., Jeong, H.J., Bae, Y.J., Park, S.Y., Kim, E., Kang, S.Y., Oh, E.S., Kim, K.J., Jeon, B., Kim, S.E., Cho, Z.H., Kim, Y.B., 2016. Loss of substantia nigra hyperintensity on 7 tesla mri of parkinson's disease, multiple system atrophy, and progressive supranuclear palsy. Parkinsonism Relat. Disord. 26, 47–54. https://doi.org/10.1016/j.parkreldis.2016.01.023.
Langkammer, C., Pirpamer, L., Seiler, S., Deistung, A., Schweser, F., Franthal, S., Homayoon, N., Katschnig-Winter, P., Koegl-Wallner, M., Pendl, T., Stoegerer, E.M., Wenzel, K., Fazekas, F., Ropele, S., Reichenbach, J.R., Schmidt, R., Schwingenschuh, P., 2016. Quantitative susceptibility mapping in Parkinson's disease. PLoS ONE 11, e0162460. https://doi.org/10.1371/journal.pone.0162460.
Lee, J.H., Baek, S.Y., Song, Y., Lim, S., Lee, H., Nguyen, M.P., Kim, E.J., Huh, G.Y., Chun, S.Y., Cho, H., 2016. The neuromelanin-related T2* contrast in postmortem human substantia nigra with 7T MRI. Sci. Rep. 6, 32647. https://doi.org/10.1038/srep32647.
Lehericy, S., Bardinet, E., Poupon, C., Vidailhet, M., Francois, C., 2014. 7 Tesla magnetic resonance imaging: a closer look at substantia nigra anatomy in Parkinson's disease. Mov. Disord. 29, 1574–1581. https://doi.org/10.1002/mds.26043.
Litvan, I., Agid, Y., Calne, D., Campbell, G., Dubois, B., Duvoisin, R.C., Goetz, C.G., Golbe, L.I., Grafman, J., Growdon, J.H., Hallett, M., Jankovic, J., Quinn, N.P., Tolosa, E., Zee, D.S., 1996. Clinical research criteria for the diagnosis of progressive supranuclear palsy (Steele-Richardson-Olszewski syndrome): report of the NINDS-SPSP international workshop. Neurology 47, 1–9.
Liu, M., Liu, S., Ghassaban, K., Zheng, W., Dicicco, D., Miao, Y., Habib, C., Jazmati, T., Haacke, E.M., 2016. Assessing global and regional iron content in deep gray matter as a function of age using susceptibility mapping. J. Magn. Reson. Imaging 44, 59–71. https://doi.org/10.1002/jmri.25130.
Liu, S., Mok, K., Neelavalli, J., Cheng, Y.C., Tang, J., Ye, Y., Haacke, E.M., 2014. Improved MR venography using quantitative susceptibility-weighted imaging. J. Magn. Reson. Imaging 40, 698–708. https://doi.org/10.1002/jmri.24413.
Mahlknecht, P., Krismer, F., Poewe, W., Seppi, K., 2017. Meta-analysis of dorsolateral nigral hyperintensity on magnetic resonance imaging as a marker for Parkinson's disease. Mov. Disord 32, 619–623. https://doi.org/10.1002/mds.26932.
Massey, L.A., Miranda, M.A., Al-Helli, O., Parkes, H.G., Thornton, J.S., So, P.W., White, M.J., Mancini, L., Strand, C., Holton, J., Lees, A.J., Revesz, T., Yousry, T.A., 2017. 9.4 T MR microscopy of the substantia nigra with pathological validation in controls and disease. Neuroimage Clin. 13, 154–163. https://doi.org/10.1016/j.nicl.2016.11.015.
Nam, Y., Gho, S.M., Kim, D.H., Kim, E.Y., Lee, J., 2017. Imaging of nigrosome 1 in substantia nigra at 3T using multiecho susceptibility map-weighted imaging (SMWI). J. Magn. Reson. Imaging 46, 528–536. https://doi.org/10.1002/jmri.25553.
Pavese, N., Tai, Y.F., 2018. Nigrosome imaging and neuromelanin sensitive MRI in diagnostic evaluation of Parkinsonism. Mov. Disord. Clin. Pract. 5, 131–140. https://doi.org/10.1002/mdc3.12590.
Postuma, R.B., Berg, D., Stern, M., Poewe, W., Olanow, C.W., Oertel, W., Obeso, J., Marek, K., Litvan, I., Lang, A.E., Halliday, G., Goetz, C.G., Gasser, T., Dubois, B., Chan, P., Bloem, B.R., Adler, C.H., Deuschl, G., 2015. MDS clinical diagnostic criteria for Parkinson's disease. Mov. Disord. 30, 1591–1601. https://doi.org/10.1002/mds.26424.
Reiter, E., Mueller, C., Pinter, B., Krismer, F., Scherfler, C., Esterhammer, R., Kremser, C., Schocke, M., Wenning, G.K., Poewe, W., Seppi, K., 2015. Dorsolateral nigral hyperintensity on 3.0T susceptibility-weighted imaging in neurodegenerative Parkinsonism. Mov. Disord. 30, 1068–1076. https://doi.org/10.1002/mds.26171.
Schmidt, M.A., Engelhorn, T., Marxreiter, F., Winkler, J., Lang, S., Kloska, S., Goelitz, P., Doerfler, A., 2017. Ultra high-field swi of the substantia nigra at 7T: reliability and consistency of the swallow-tail sign. BMC Neurol. 17, 194. https://doi.org/10.1186/s12883-017-0975-2.
Schwarz, S.T., Afzal, M., Morgan, P.S., Bajaj, N., Gowland, P.A., Auer, D.P., 2014. The 'swallow tail' appearance of the healthy nigrosome - a new accurate test of Parkinson's disease: a case-control and retrospective cross-sectional MRI study at 3T. PLoS One 9, e93814. https://doi.org/10.1371/journal.pone.0093814.
Schwarz, S.T., Mougin, O., Xing, Y., Blazejewska, A., Bajaj, N., Auer, D.P., Gowland, P., 2018. Parkinson's disease related signal change in the nigrosomes 1-5 and the substantia nigra using T2* weighted 7T MRI. Neuroimage Clin. 19, 683–689. https://doi.org/10.1016/j.nicl.2018.05.027.
Sung, Y.H., Lee, J., Nam, Y., Shin, H.G., Noh, Y., Shin, D.H., Kim, E.Y., 2018. Differential involvement of nigral subregions in idiopathic Parkinson's disease. Hum. Brain Mapp. 39, 542–553. https://doi.org/10.1002/hbm.23863.
Tang, J., Liu, S., Neelavalli, J., Cheng, Y.C., Buch, S., Haacke, E.M., 2013. Improving susceptibility mapping using a threshold-based K-space/image domain iterative reconstruction approach. Magn. Reson. Med. 69, 1396–1407. https://doi.org/10.1002/mrm.24384.
Thenganatt, M.A., Jankovic, J., 2014. Parkinson disease subtypes. JAMA Neurol. 71, 499–504. https://doi.org/10.1001/jamaneurol.2013.6233.
Vos, T., A.C., Arora M, Barber, R.M., Bhutta, Z.A., Brown, A., 2016. Global, regional, and national incidence, prevalence, and years lived with disability for 310 diseases and injuries, 1990-2015: a systematic analysis for the global burden of disease study 2015. Lancet 388, 1545–1602. https://doi.org/10.1016/S0140-6736(16)31678-6.
Zecca, L., Casella, L., Albertini, A., Bellei, C., Zucca, F.A., Engelen, M., Zadlo, A., Szewczyk, G., Zareba, M., Sarna, T., 2008. Neuromelanin can protect against iron-mediated oxidative damage in system modeling iron overload of brain aging and Parkinson's disease. J. Neurochem. 106, 1866–1875. https://doi.org/10.1111/j.1471-4159.2008.05541.x.
Zecca, L., Gallorini, M., Schunemann, V., Trautwein, A.X., Gerlach, M., Riederer, P., Vezzoni, P., Tampellini, D., 2001. Iron, neuromelanin and ferritin content in the substantia nigra of normal subjects at different ages: consequences for iron storage and neurodegenerative processes. J. Neurochem. 76, 1766–1773.
Zecca, L., Stroppolo, A., Gatti, A., Tampellini, D., Toscani, M., Gallorini, M., Giaveri, G., Arosio, P., Santambrogio, P., Fariello, R.G., Karatekin, E., Kleinman, M.H., Turro, N., Hornykiewicz, O., Zucca, F.A., 2004. The role of iron and copper molecules in the neuronal vulnerability of locus coeruleus and substantia nigra during aging. Proc. Natl. Acad. Sci. U S A 101, 9843–9848. https://doi.org/10.1073/pnas.0403495101.
Zhang, Z.X., Roman, G.C., Hong, Z., Wu, C.B., Qu, Q.M., Huang, J.B., Zhou, B., Geng, Z.P., Wu, J.X., Wen, H.B., Zhao, H., Zahner, G.E., 2005. Parkinson's disease in China: prevalence in Beijing, Xian, and Shanghai. Lancet 365, 595–597. https://doi.org/10.1016/S0140-6736(05)17909-4.
Zucca, F.A., Segura-Aguilar, J., Ferrari, E., Munoz, P., Paris, I., Sulzer, D., Sarna, T., Casella, L., Zecca, L., 2017. Interactions of iron, dopamine and neuromelanin pathways in brain aging and Parkinson's disease. Prog. Neurobiol. 155, 96–119. https://doi.org/10.1016/j.pneurobio.2015.09.012.